

# 1 Structural characterization of NORAD reveals a stabilizing role of 2 spacers and two new repeat units.

3 Uciel Chorostecki<sup>1,2</sup>, Ester Saus<sup>1,2</sup>, and Toni Gabaldón<sup>1,2,3\*</sup>

4

5 1) Barcelona Supercomputing Centre (BSC-CNS). Jordi Girona, 29. 08034. Barcelona, Spain.

6 2) Institute for Research in Biomedicine (IRB Barcelona), The Barcelona Institute of Science and  
7 Technology, Baldiri Reixac, 10, 08028 Barcelona, Spain

8 3) Catalan Institution for Research and Advanced Studies (ICREA), Barcelona, Spain

9 \*Author for correspondence: [toni.gabaldon@bsc.es](mailto:toni.gabaldon@bsc.es)

10

## 11 Abstract

12 Long non-coding RNAs (lncRNAs) can perform a variety of key cellular functions by interacting  
13 with proteins and other RNAs. Recent studies have shown that the function of lncRNAs are  
14 largely mediated by their structures. However, our structural knowledge for most lncRNAs is  
15 limited to sequence-based computational predictions. Non-coding RNA activated by DNA  
16 damage (NORAD) is an atypical lncRNA due to its abundant expression and high sequence  
17 conservation. NORAD regulates genomic stability by interacting with proteins and microRNAs.  
18 Previous sequence-based characterization has identified a modular organization of NORAD  
19 composed of several NORAD repeat units (NRUs). These units comprise the protein-binding  
20 elements and are separated by regular spacers of unknown function. Here, we experimentally  
21 determine for the first time the secondary structure of NORAD using the nextPARS approach.  
22 Our results suggest that the spacer regions provide structural stability to NRUs. Furthermore,  
23 we uncover two previously-unreported NRUs, and determine the core structural motifs  
24 conserved across NRUs. Overall, these findings will help to elucidate the function and evolution  
25 of NORAD.

26

27

## 28 Keywords

29 long non-coding RNAs, NORAD, RNA structure, Probing RNA, ncRNAs

30

## 31 Introduction

32 Long non-coding RNAs (lncRNAs) constitute a heterogeneous family of RNA transcripts defined  
33 by their length (> 200 nucleotides (nt)), and their lack of protein-coding potential. Most lncRNAs  
34 are expressed at low levels and in a tissue- or cell type-specific manner, and are poorly  
35 conserved both at the sequence and exon-intron structure levels [1,2]. Over the last years, an  
36 increasing number of lncRNAs have been associated with a variety of cellular and  
37 developmental functions [3–5], and have been shown to be altered in various human diseases  
38 [6]. However, the functions and structures of the vast majority of lncRNAs, remain poorly  
39 understood.

40 lncRNAs can form complex secondary structures, which tend to be more conserved  
41 than primary sequences and are thought to mediate their biological functions [7,8]. However,  
42 controversy remains as to whether secondary structures of lncRNAs are evolutionarily  
43 conserved [9]. Although molecular probing techniques allow assessing RNA structures folded *in*  
44 *vitro*, the large size of many lncRNAs poses a significant challenge. As a result, only a few  
45 lncRNA structures have been experimentally characterized *in vitro* [9], including those of  
46 HOTAIR [10], RepA [11], Xist [12,13], ncSRA [14], and lincRNAp21 [14,15].

47 Many sequences, including riboswitches, mRNAs and long non-coding RNAs [9], are  
48 expected to fold into a variety of competing structures that can coexist. To account for this  
49 structural diversity, several methods have been recently developed that allow to study  
50 alternative RNA conformations using experimental data [16–20].

51 The non-coding RNA activated by DNA damage (NORAD) is a 5.3 kilobases (kb) long  
52 lncRNA that is widely expressed and conserved across mammals. Previous sequence analyses  
53 of this lncRNA have described the presence of several repeated elements - NORAD repeat  
54 units or NRUs - that are predicted to fold into similar secondary structures and tend to be  
55 conserved [21,22]. NORAD maintains genomic stability by sequestering RNA-binding PUMILIO  
56 proteins (PUM1 and PUM2), thereby preventing them from interacting with their targets [21].  
57 PUMILIO proteins act by repressing the translation of specific target mRNAs by binding to  
58 PUMILIO response elements (PRE) present in their 3' untranslated region (3'UTR) [23]; [23,24].  
59 In the absence of NORAD, PUMILIO proteins drive chromosomal instability caused by DNA  
60 repair, hyperactively repressing mitotic, and DNA replication factors [21].

61 In addition, NORAD acts as a competitive endogenous RNA (ceRNA) and regulates  
62 cancer progression by sponging MicroRNAs (miRNAs) [25,26]. MiRNAs are small regulatory  
63 RNAs of about ~20 nt in length that play critical regulatory roles in eukaryotic cells where they  
64 mediate post-transcriptional silencing of specific genes [27–29].

65 Despite the increasing relevance and known functions of NORAD, the empirical  
66 characterization of its structure is still lacking. To shed light on the function and evolution of  
67 NORAD, we here characterized its secondary structure using experimental probing with the  
68 nextPARS approach [30]. In addition, we assessed how changes in sequence context and shifts  
69 in temperature impact the structure of NRUs and other relevant NORAD motifs. Our results  
70 provide evidence that the spacer sequences provide structural stability to NRUs and that the  
71 structure around conserved SAM68-binding sites is more robust to thermal shifts than other

positions in the NORAD sequence. Finally, we define the core structural motifs conserved across NRUs, and uncover the presence of two previously-unreported NRUs.

## Materials and Methods

### Sample preparation

The structure of several NORAD fragments was experimentally probed using nextPARS (PMID: 29358234) at three different temperatures (23 °C, 37 °C and 55 °C) by spiking the fragments of interest into fungal total or polyA+ RNA samples.

The probed NORAD fragments were the following: three RNA fragments covering the full-length NORAD lncRNA (called NORAD#1, NORAD#2 and NORAD#3, overlapping 1903, 1862 and 1614 bases, respectively), and 11 NORAD repetitive units previously described [22] with their surrounding regions (NRU#1, NRU#2, NRU#3, NRU#4, NRU#6, NRU#7, NRU#8, NRU#9, NRU#10, NRU#11 and NRU#12, overlapping 179 nt each) [Supplementary table S1]. To produce these fragments, NORAD was cloned into the pUC57 vector by GenScript Biotech (Netherlands). The plasmid was transformed in DH5α *E. coli* competent cells previously prepared in our lab according to manufacturer's instructions (Mix & Go *E. coli* Transformation Kit & Buffer Set, ZymoResearch). Single colonies were grown in LB+Ampicillin medium (37 °C, 220 rpm, overnight), and plasmids were purified using QIAprep Spin Miniprep kit according to the manufacturer's instructions (Qiagen). PCRs were performed to amplify and linearize the different NORAD fragments using the Pfu mix (#2021, DongSheng Biotech) and a 0.4 μM final concentration of each primer (forward and reverse) in a total volume of 40 μl. Supplementary Table S1 shows primer sequences and amplicon sizes and Supplementary Table S2 specifies PCR conditions used per each fragment. PCR amplicons were purified using a QIAquick PCR purification kit according to the manufacturer's instructions (Qiagen) and then they were Sanger sequenced, to confirm that no mutation had been introduced in the fragments of interest. Then, all NORAD fragments already linearized were transcribed *in vitro* using the T7 RiboMax Large-scale RNA production system according to the manufacturer's instructions (Promega). Finally, RNAs of interest were size-selected and purified using Novex-TBE Urea gels according to the manufacturer's instructions (Life Technologies). Final quality control of the purified RNAs was performed using the Agilent 2100 Bioanalyzer with the RNA 6000 Pico LabChip Kit (Agilent) and the Qubit Fluorometer with the Qubit RNA BR (Broad-Range) Assay Kit (ThermoFisher Scientific). Ten other RNA molecules were spiked into the samples (TETp4p6, TETp9-9.1, hSRA, mSRA, ROX2, GAS5, HOTAIR\_NCBIBI\_RINN, 372\_BRAVEHEART, 373\_BRAVEHEART, B2 and U1) [Supplementary table S3]

### Secondary structure probing with NextPARS

For the enzymatic probing of RNA samples at different temperatures (23 °C, 37 °C and 55 °C), we used the nextPARS protocol [30], adapting it when necessary for the probing at higher temperatures. Briefly, 2 μg of PolyA+ RNA or total RNA were mixed with 20 ng of each NORAD RNA fragment and were brought to a final volume of 80 μl with nuclease-free water. Samples

were first denatured at 90 °C for 2 min and immediately cooled down to 4 °C on ice for 2 min. Then, 10 µl of ice-cold 10X RNA structure buffer (Ambion) were added to the samples and mixed by pipetting up and down several times. When probing at 23 °C, RNA samples were subsequently brought from 4 °C to 23 °C, in about 20 min (1 °C per min). For samples probed at 37 °C and 55 °C, the temperature was brought from 4 °C to 30 °C (1 min per each °C), samples were incubated 5 min at 30 °C, and then brought to 37 °C and 55 °C, respectively, for enzymatic digestion. Finally, 10 µl of the corresponding dilutions of RNase V1 (Ambion), S1 nuclease (Fermentas), or nuclease-free water were added to the V1-digested, S1-digested and undigested samples, respectively. The enzyme concentration used was different depending on the probing temperature, to compensate for the effect of higher temperatures to prevent over-digestion of the RNA samples and according to previous studies [31]. Thus, the final reaction contained 0.03 U, 0.015 U or 0.0075 U of RNase V1, and 200 U, 100 U or 50 U of S1 nuclease for samples probed at 23 °C, 37 °C or 55 °C, respectively. After mixing by pipetting, samples were incubated at each corresponding temperature for 15 minutes more. The RNAs were purified using RNeasy MiniElute Cleanup kit following the manufacturer's instructions (Qiagen). Quality controls with NanoDrop 1000 Spectrophotometer (Thermo Scientific) and Agilent 2100 Bioanalyzer with the RNA 6000 Pico LabChip® Kit (Agilent) were performed before and after the digestion, to confirm that samples were not digested with the initial denaturation or over-digested after the enzymatic treatment.

### **Library preparation and sequencing.**

We used the TruSeq Small RNA Sample Preparation Kit (Illumina) to prepare the libraries for further sequencing. We initially performed a phosphatase treatment incubating 16 µl of the digested samples for 30 min at 37 °C and 5 min at 65 °C mixed with 2.5 µl of 10X phosphatase buffer, 2.5 µl of nuclease-free water, 1 µl of RNase inhibitor and 3 µl of Antarctic phosphatase (New England BioLabs Inc.). We then performed a kinase treatment adding 4 µl of T4 Polynucleotide Kinase (PNK, New England BioLabs Inc.), 5 µl of 10X PNK buffer, 10 µl of ATP 10 mM, 1 µl of RNase inhibitor and nuclease-free water up to a total volume of 50 µl, and incubating the samples 1 hour at 37 °C. Samples were then purified using RNeasy MiniElute Cleanup kit following manufacturer's instructions (Qiagen) with a 10 µl RNase-free water final elution step. Samples were concentrated using a centrifugal evaporator Speed Vac® to a final volume of 5 µl and we started the TruSeq Small RNA Sample Preparation Kit (Illumina) protocol according to manufacturer's instructions. After the final purification of the cDNA libraries, we performed quality control of each library using Agilent 2100 bioanalyzer with the DNA 1000 Kit (Agilent). Libraries were sequenced in single-reads with read lengths of 50 nucleotides in Illumina HiSeq2500 sequencers at the Genomics Unit of the CRG.

### **Computation of the nextPARS scores**

The computation of the nextPARS scores was obtained following the protocol in [30,32]. Briefly, we removed adapters with cutadapt and mapped the reads using STAR [33]. Then, we used in-house scripts for parsing the mapped reads and retrieved the 5' -end position in the NORAD

transcript. This results in a digestion profile that indicates the number of cuts per position of the transcript. To obtain the scores from nextPARS probing experiments we used as an input the digestion profile. The output contains a structural profile of the NORAD transcript (single-or double-stranded state), with a score for each nucleotide that ranges from -1.0 (highest preference for single strand) to 1.0 (highest preference for double-strand) ([https://github.com/Gabaldonlab/nextPARS\\_docker](https://github.com/Gabaldonlab/nextPARS_docker)).

## **RNA secondary structure prediction and visualization.**

To obtain the secondary structure of NORAD and NRUs we use RNAstructure software [34]. Using nextPARS2SHAPE v1.0 script (<https://github.com/Gabaldonlab/MutiFolds/>) we converted nextPARS score to SHAPE-like normalized reactivities that were used to provide pseudoenergy restraints to the Fold software. The consensus structure models have been generated using the R2R software [35]. RNA structures were constructed using VARNA (Version 3-93) [36].

## **Identification of repetitive units in NORAD**

To identify new repetitive elements in NORAD we first performed a multiple sequence alignment with T-Coffee (Version\_11.00.8cbe486) [37] using the regions of the 12 described NRUs. Then, a covariance model (CM) was built using Infernal 1.1.3. [38] cmbuild on the 12 NRUs sequences with --noss parameter to ignore the secondary structure annotation. Then, we calibrated the CM with cmcalibrate. Next, cmsearch was used to search for the CM against NORAD and the 14 sequences below the E-value cutoff (0.01) were retrieved.

## **Prediction of multiple folding conformations, guided by nextPARS data.**

Rsample (Version 6.2) [19] was used to calculate the partition function for the NRUs from NORAD sequence to determine the multiple conformations. To perform a complete Rsample calculation, we performed the following steps. First, we converted the nextPARS score to SHAPE-like reactivities and then we ran Rsample using the SHAPE-like constraint to produce a Partition Save File (PFS). After that, we ran stochastic, using this PFS file as input, and we created a CT file with Boltzmann ensemble of 1,000 structures. Finally using the R script from Rsample (RsampleCluster.R) we use the CT file to calculate the optimal number of clusters and their centroids to model the NRUs sequences that populate multiple structures, including the relative probabilities of those structures. To evaluate conserved structural elements within the ensemble of structures of the NRUs, we used the Beagle (BEar Alignment Global and Local) software [39]. We performed an all-vs-all alignment for all the NRUs to identify common secondary structures and compared them with the most stable structure.

## **Statistical methods**

Statistics were performed using Wilcoxon rank-sum and Kruskal-Wallis tests. The similarity of nextPARS scores between the same residues in NRU segments folded independently or within



each piece and larger NORAD fragments was measured by Pearson's correlation. The Gardner-Altman estimation plots were produced using the python version of dabest [40].

## Deposited data

Raw sequencing data of nextPARS experiments were deposited in the Sequence Read Archive under the BioProject ID PRJNA714002. (Reviewer's access <https://dataview.ncbi.nlm.nih.gov/object/PRJNA714002?reviewer=c05bml4s9go209k1vvhhs4pe> s7).

## Results

### Structural characterization of NORAD

Resolving the structure of NORAD *in vitro* is exceptionally challenging because of the large size of this transcript. To circumvent this problem, we synthesized, cloned, and *in vitro* transcribed (see Materials and Methods) three overlapping NORAD fragments [Fig. 1A], and subsequently subjected them to enzymatic probing using the nextPARS method [30]. This approach renders single-nucleotide resolution measurements of *in vitro* secondary structure, which can be represented by a structural profile (single- or double-stranded state), providing a score for each residue, ranging from -1.0 (highest preference for single strand) to 1.0 (highest preference for double-strand). We converted the nextPARS score to SHAPE-like reactivity and used this to provide constraints for secondary structure prediction [Fig. 1B]. Our results show that most of the NRUs form independently-folded structures (NRU#2, NRU#3, NRU#5, NRU#7, NRU#8, NRU#9, NRU#11 and NRU#12) but some of them seem to interact with each other or with other NORAD regions [Fig. 1B].

To analyze NRUs structures in detail, and to assess the effect of the NORAD sequence context in NRU folding, we designed non-overlapping 179 nt long fragments covering 11 of the 12 previously described NRUs [22] and performed nextPARS experiments [Fig. 1A]. To identify structural subdomains in NORAD, we followed a strategy previously used with HOTAIR [10,41]. In this approach, the full-length lncRNA profile is compared to the profiles of individual RNA segments to identify potential independently-folded sub-domains. Comparing the nextPARS profile of the NRUs with the same sequence in the context of the full NORAD molecule, shows a high correlation, with a p-value < 0.01 [Supplementary Figure S1]. Pearson's correlation coefficient values ( $\rho$ ) are expected to be higher for fragments that do not break elements of the secondary structure observed in the full-length molecule. This was the case for the eleven NRUs analyzed ( $\rho > 0.8$ ). Correlations values were particularly high ( $\rho > 0.9$ ) for some of the NRUs (NRU#1, NRU#4, NRU#8, NRU#10 and NRU#12), suggesting that these regions form more stable local structures [Supplementary Figure S1].

### Spacer sequences provide structural stability to NRUs.

To evaluate the robustness and stability of NORAD secondary structure, we performed nextPARS experiments at three different temperatures: 23 °C, 37 °C and 55 °C to study the alterations prompted by these temperature shifts as a means of structural perturbation [Fig. 2A]. We compared nextPARS scores obtained in equivalent residues when probed in NRU-specific fragments or in larger NORAD fragments, and when probed at different temperatures in the context of the two molecular sizes. On average, the correlation between secondary structures was higher across varying temperatures than when NRUs structures were compared between those folded in isolated fragments with larger NORAD fragments [Fig. 2A,B]. These results suggest that the molecular context provided by the surrounding NORAD spacer sequences has a larger influence on the structure of NRU than sharp shifts in temperature.

Then, we measured the stability of NRUs by averaging the standard deviation of nextPARS scores at different temperatures [Fig. 2C]. Importantly, we observed that structural variability across temperatures was higher in NRUs fragments compared to larger NORAD fragments, supporting a stabilizing role of the molecular context when NRUs are embedded within larger NORAD fragments [Fig. 2C]. To ensure that the observed structural variability differences are not due to the effect of sequence length (i.e. longer molecules having higher stabilities), we use the information of nextPARS experiments of ten RNA molecules that were spiked with NORAD samples, with variable size [30], and measured the structural stability at different temperatures. Our results did not detect any statistically significant correlation between stability and sequence length [Supplementary Figure S2], suggesting our results cannot simply be attributed to differences in length between NRU-specific, and larger NORAD fragments.

### **Conserved SAM68-binding sites in NORAD are particularly robust to structural perturbation by temperature shift.**

SAM68 (KHDRBS1) is an RNA-binding protein (RBP) that performs several functions in the nucleus and cytoplasm [42]. It is required for efficient recruitment of PUMILIO2 protein (PUM2) to NORAD and the regulation of Pum activity by NORAD [43–45]. SAM68 recognizes UAAA motifs [46], which in NORAD are present in 16 motif pairs separated by linkers of 15-35 bases. These motifs show higher evolutionary conservation as compared to the rest of the NORAD sequence [43]. When comparing nextPARS score variability at different temperatures for NRU-specific fragments in positions of UAAA motifs to other positions of NRUs, we observed that the motif sites were less variable as compared to the remaining residues in the NRUs (p-value = 0.010148) [Fig. 3A]. To further investigate the association between sequence conservation and structural flexibility in UAAA motifs, we measured the correlation between the evolutionary conservation as estimated by the PhyloP score (based on the 100-way vertebrate alignment) and the variability of structural profiles in the position of all UAAA motifs. First, we measured the structural variability of the UAAA motifs using the nextPARS probing data from NRU-specific fragments and found no significant correlation between the level of conservation and the amount of structural variability [Fig. 3B]. Then, we calculated the same measure of correlation but using the nextPARS data from the larger NORAD fragments and observed a significant negative correlation between sequence conservation and structural variability within UAAA sites- the higher the sequence conservation, the lower the structural variability at these

positions - [Fig. 3B]. We obtained similar results using PhastCons score or PhyloP score at different conservation levels [Fig. 3B]. These results suggest that SAM68-binding sites (UAAA motif) are robust to structural perturbation by temperature shift.

## **Considering structural diversity of NRUs to study functional and evolutionary relationships.**

We next set out to investigate other NORAD conserved elements beyond the known protein binding sites. We used our empirical data to study the two previously predicted hairpin structures present in the NRUs core, as such conserved secondary structure motifs are rarely detectable in lncRNAs [22]. We produced a multiple sequence alignment to derive a consensus secondary structure from the eight NRUs displaying a clear conserved long stem-loop hairpin [43] (NRU#1, NRU#3-8 and NRU#10). In the predicted consensus structure [Fig. 4A], we observed a short stem-loop structure comprising four paired bases and a variable loop followed by a second large stem-loop structure with nine base pairs.

Many sequences including mRNA, lncRNAs and riboswitches are expected to fold in multiple, coexisting structures [9]. To investigate this in the case of NORAD, we used Rsample [19] in combination with nextPARS data to predict the presence of alternative RNA structures for NRUs, and studied these conformations. NRU#2 was one of the four NRUs that was excluded from the analysis of the consensus structure, as this unit did not contain most of the repeat motifs in comparison to the rest of the NRUs [22]. When we predicted the structure of NRU#2, we observed that it was folded in two alternative conformations. The major conformation (inferred to represent 84.1% of the molecules in the mix) was predicted to form a large stem-loop after a U-rich stretch, and a small stem-loop before that U-rich [Fig. 4B]. These detected structure motifs were similar to the ones detected in some of the characterized NRUs (NRU#1, NRU#3-8 and NRU#10) [22]. In contrast, in the minor conformation (15.9%) or in the computationally predicted conformation, we could not detect the combination of sequence and structure motifs present in the other NRUs that were previously characterized [Fig. 4B and Supplementary Figure S3A]. This indicates that considering the possibility of competing structural conformations enhances our ability to detect structural similarity that is otherwise missed by standard approaches based on a single stable structure.

Then, we searched for shared structurally related regions among the different NRUs, considering alternative conformations. For that purpose, we used the Beagle software [39] to perform an all versus all comparison of the most stable structure in all NRUs fragments. Then, we did the same all versus all comparisons but using the complete ensemble of alternative structures. We observed that the structural similarity (z-score) was higher for the ensemble of structures, as compared with the most stable one ( $p$ -value = 0.00095) [Fig. 4C], meaning again that using the alternative structures that may coexist within NORAD could be more accurate than using only the most stable one.

## **Discovery of two previously uncharacterized NRUs.**

Previous comparison of human NORAD sequences revealed that this lncRNA could be decomposed into at least 12 repeating units of ~300 nt each [43]. When we studied the relative



positions of the core sequence of the NRUs throughout NORAD, we noticed that consecutive units were separated by a sequence spacers of similar length (between ~270 nt and ~340 nt), with the exception of NRU#10 and NRU#11, which were separated by ~900 nt [Fig. 5A]. To investigate the presence of novel NRUs, we used infernal [38] to derive a model for NRUs (see Materials and Methods). Using this model on NORAD, we identified the 12 known NRUs, as expected, but we also detected the presence of two additional NRUs that we termed NRU#10a and NRU#10b. Interestingly, these units appear within the unusually long intervening region between NRU#10 and NRU#11 and are separated by the approximately same distance as the rest of the NRUs [Fig. 5A]. Multiple sequence alignment of the core sequences of the known and newly identified NRUs showed a high degree of sequence similarity [Supplementary figure S4A]. Furthermore, we noticed a common sequence motif located at ~50 nt downstream of the end of the core of NRU#10a and other NRUs. [Supplementary figure S4B]. Moreover, in the new NRUs, we could identify most of the sequence and structure motifs typical for known NRUs, including the presence of SAM68-binding sites within the NRU or nearby [Fig. 5B] [43].

Finally, we assessed whether the structure of the newly discovered NRUs was similar to the previously characterized ones, but aligning them to the previously mentioned alignment of the eight structurally conserved NRUs (NRU#1, NRU#3-8 and NRU#10). We were able to obtain a new consensus structure with the same short stem-loop structure but the consensus large stem-loop was smaller compared with the consensus structure without the new NRUs [Supplementary Figure S5A], suggesting that part of the consensus structure is not present in the newly identified NRUs. However, the structural similarity to the canonical consensus seems larger than that of NRU#2 and NRU#9. Based on these results, we conclude that the two newly identified NRU correspond to bona-fide functional elements in NORAD, and should be considered in future research.

## Discussion

NORAD is a critical regulator of genome stability. Moreover, human NORAD is dysregulated in various types of cancer and could be an excellent diagnostic or therapeutic biomarker in tumour cells [26]. Since lncRNAs have no protein-coding potential, their structure may be key for exploring their functionality. Despite this, there have been no studies of the *in vitro* structurome of NORAD. To fill this important gap, we performed nextPARS experiments that allowed us to study heat- or context-induced structural changes in NORAD at a single-nucleotide resolution. Moreover, we experimentally determined the *in vitro* secondary structure of NORAD and defined the core structural motifs conserved across NRUs. We identified two previously uncharacterized NRUs within an unusually long linker region. The addition of the two newly discovered NRUs results in all core units distributed along the whole NORAD sequence and placed at very regular distances. A possible explanation for this could be that the hairpin elements in the NRUs are interacting with each other or that they help to position the protein-binding sites at an advantageous distance from each other. We noticed that the NRU#10a was less conserved in their sequence compared to NRU#10b and the rest of the NRUs and, in contrast to the case of

NRU#10b, we could not identify a putative SAM68-binding site sequence near the NRU#10a core.

The repetitive and modular nature of NORAD sequence allowed us to study several fragments at once and simplify the task of studying the structure of this long RNA transcript in its entirety. Our results indicate a stabilizing role of spacer sequences between NRUs, with their effect on the structure being larger than sharp shifts in temperature. How spacers stabilize NRUs is unclear. One possibility is that they favor interactions with other NRUs by placing them at some optimal distance, which would explain the regularity in spacer lengths. Alternatively, they may interact with some parts of the NRU structure, providing some additional stability. An RNA could fold in different structures inside the cell and many conformations for the same RNA coexist in equilibrium. Both for isolated NRUs and larger NORAD fragments experiments we observed that many sites exhibit clear signals for both single- and double-strand specific enzymes (nextPARS score near zero) which may result from noise, but also from the actual co-existence of alternative secondary structures during the experiment. Taking this into account, we estimated and compared the structural conformations of two NRUs and we detected structure motifs that were omitted when using the more stable structure. We revealed that these motifs were similar to the ones detected in some of the known NRUs. Moreover, we showed the importance of considering the ensemble of structures to compare structural elements in NRUs. Furthermore, a similar approach could be used to look for shared structural elements between different species to study the evolution of NORAD.

NORAD contains several SAM68-binding sites (UAAA motif) and the interaction between NORAD and the RNA-binding protein SAM68 is required for NORAD function. We compared the nextPARS data at different temperatures to evaluate the stability of SAM68-binding sites motif secondary structure. We revealed that positions of UAAA motifs were more robust to thermal shifts than other positions in the NRUs sequence. Interestingly, we observed a correlation between conservation and flexibility in UAAA motifs but only when we use nextPARS data from larger NORAD fragments experiments and not when using data from NRU-specific fragments.

For certain small RNAs, the *in vitro* folding landscape can recapitulate effectively the *in vivo* one, while for long RNAs the structures sometimes differ *in vitro* versus *in vivo* [47,48]. These differences are mainly due to interactions with other molecules. *In vivo* structure probing may provide more accurate information on biologically relevant RNA structures [49,50]. In this work, we use only information from *in vitro* experiments, but we think that one future perspective could be the combination of these two experimental methods for obtaining the full picture of the RNA structurome. Nonetheless, both *in vitro* and *in vivo* approaches have limitations [51]. Furthermore, NORAD has sponge potential on several miRNAs and some of them were validated in different studies. Another future perspective could be to study the secondary structure of miRNA binding sites. We hypothesize that NORAD structure could modulate miRNA cleavage by facilitating or preventing accessibility of the miRNA to its binding site.

Taken together, our analyses contribute important novel insights into the structural organization of NORAD. Future studies should focus on determining how the different structural elements of NORAD interact with each other and with other molecules, and how different mutations may affect these interactions and the functions mediated by them. Only by understanding the complex relationships between, sequence, structure, and function will we be able to comprehend the roles of NORAD in the normal functioning of the cell and in diseases

such as cancer. Eventually, this may open the door to design novel therapeutic strategies in the fight against cancer.

## Acknowledgements

UC was funded in part through H2020 Marie Skłodowska-Curie Actions (H2020-MSCA-IF-2017-793699) and MICINN (IJC2019-039402-I). TG group acknowledges support from the Spanish Ministry of Science and Innovation for grant PGC2018-099921-B-I00, cofunded by European Regional Development Fund (ERDF); from the Catalan Research Agency (AGAUR) SGR423; from the European Union's Horizon 2020 research and innovation programme (ERC-2016-724173); from the Gordon and Betty Moore Foundation (Grant GBMF9742) and from the Instituto de Salud Carlos III (INB Grant PT17/0009/0023 - ISCIII-SGEFI/ERDF).

## References

- [1] T. Derrien, R. Johnson, G. Bussotti, A. Tanzer, S. Djebali, H. Tilgner, G. Guernec, D. Martin, A. Merkel, D.G. Knowles, J. Lagarde, L. Veeravalli, X. Ruan, Y. Ruan, T. Lassmann, P. Carninci, J.B. Brown, L. Lipovich, J.M. Gonzalez, M. Thomas, C.A. Davis, R. Shiekhattar, T.R. Gingeras, T.J. Hubbard, C. Notredame, J. Harrow, R. Guigó, The GENCODE v7 catalog of human long noncoding RNAs: analysis of their gene structure, evolution, and expression, *Genome Res.* 22 (2012) 1775–1789. <https://doi.org/10.1101/gr.132159.111>.
- [2] J.J. Quinn, H.Y. Chang, Unique features of long non-coding RNA biogenesis and function, *Nat. Rev. Genet.* 17 (2016) 47–62. <https://doi.org/10.1038/nrg.2015.10>.
- [3] A. Fatica, I. Bozzoni, Long non-coding RNAs: new players in cell differentiation and development, *Nat. Rev. Genet.* 15 (2014) 7–21. <https://doi.org/10.1038/nrg3606>.
- [4] L. Li, H.Y. Chang, Physiological roles of long noncoding RNAs: insight from knockout mice, *Trends Cell Biol.* 24 (2014) 594–602. <https://doi.org/10.1016/j.tcb.2014.06.003>.
- [5] I. Ulitsky, D.P. Bartel, lincRNAs: genomics, evolution, and mechanisms, *Cell.* 154 (2013) 26–46. <https://doi.org/10.1016/j.cell.2013.06.020>.
- [6] O. Wapinski, H.Y. Chang, Long noncoding RNAs and human disease, *Trends Cell Biol.* 21 (2011) 354–361. <https://doi.org/10.1016/j.tcb.2011.04.001>.
- [7] I.V. Novikova, S.P. Hennessey, C.-S. Tung, K.Y. Sanbonmatsu, Rise of the RNA machines: exploring the structure of long non-coding RNAs, *J. Mol. Biol.* 425 (2013) 3731–3746. <https://doi.org/10.1016/j.jmb.2013.02.030>.
- [8] R. Li, H. Zhu, Y. Luo, Understanding the Functions of Long Non-Coding RNAs through Their Higher-Order Structures, *Int. J. Mol. Sci.* 17 (2016). <https://doi.org/10.3390/ijms17050702>.
- [9] E. Rivas, J. Clements, S.R. Eddy, A statistical test for conserved RNA structure shows lack of evidence for structure in lncRNAs, *Nat. Methods.* 14 (2017) 45–48. <https://doi.org/10.1038/nmeth.4066>.
- [10] S. Somarowthu, M. Legiewicz, I. Chillón, M. Marcia, F. Liu, A.M. Pyle, HOTAIR forms an intricate and modular secondary structure, *Mol. Cell.* 58 (2015) 353–361. <https://doi.org/10.1016/j.molcel.2015.03.006>.

- 460 [11] F. Liu, S. Somarowthu, A.M. Pyle, Visualizing the secondary and tertiary architectural  
461 domains of lncRNA RepA, *Nat. Chem. Biol.* 13 (2017) 282–289.  
462 <https://doi.org/10.1038/nchembio.2272>.
- 463 [12] S. Maenner, M. Bland, L. Fouillen, A. Savoye, V. Marchand, A. Dubois, S.  
464 Sanglier-Cianfèrari, A. Van Dorsselaer, P. Clerc, P. Avner, A. Visvikis, C. Branlant, 2-D  
465 structure of the A region of Xist RNA and its implication for PRC2 association, *PLoS Biol.* 8  
466 (2010) e1000276. <https://doi.org/10.1371/journal.pbio.1000276>.
- 467 [13] R. Fang, W.N. Moss, M. Rutenberg-Schoenberg, M.D. Simon, Probing Xist RNA Structure  
468 in Cells Using Targeted Structure-Seq, *PLoS Genet.* 11 (2015) e1005668.  
469 <https://doi.org/10.1371/journal.pgen.1005668>.
- 470 [14] I.V. Novikova, S.P. Hennelly, K.Y. Sanbonmatsu, Structural architecture of the human long  
471 non-coding RNA, steroid receptor RNA activator, *Nucleic Acids Res.* 40 (2012) 5034–5051.  
472 <https://doi.org/10.1093/nar/gks071>.
- 473 [15] I. Chillón, A.M. Pyle, Inverted repeat Alu elements in the human lincRNA-p21 adopt a  
474 conserved secondary structure that regulates RNA function, *Nucleic Acids Res.* 44 (2016)  
475 9462–9471. <https://doi.org/10.1093/nar/gkw599>.
- 476 [16] E. Morandi, I. Manfredonia, L.M. Simon, F. Anselmi, M.J. van Hemert, S. Oliviero, D.  
477 Incarnato, Genome-scale deconvolution of RNA structure ensembles, *Nat. Methods.*  
478 (2021). <https://doi.org/10.1038/s41592-021-01075-w>.
- 479 [17] H. Li, S. Aviran, Statistical modeling of RNA structure profiling experiments enables  
480 parsimonious reconstruction of structure landscapes, *Nat. Commun.* 9 (2018) 606.  
481 <https://doi.org/10.1038/s41467-018-02923-8>.
- 482 [18] P.J. Tomezsko, V.D.A. Corbin, P. Gupta, H. Swaminathan, M. Glasgow, S. Persad, M.D.  
483 Edwards, L. McIntosh, A.T. Papenfuss, A. Emery, R. Swanstrom, T. Zang, T.C.T. Lan, P.  
484 Bieniasz, D.R. Kuritzkes, A. Tsibris, S. Rouskin, Determination of RNA structural diversity  
485 and its role in HIV-1 RNA splicing, *Nature.* 582 (2020) 438–442.  
486 <https://doi.org/10.1038/s41586-020-2253-5>.
- 487 [19] A. Spasic, S.M. Assmann, P.C. Bevilacqua, D.H. Mathews, Modeling RNA secondary  
488 structure folding ensembles using SHAPE mapping data, *Nucleic Acids Res.* 46 (2018)  
489 314–323. <https://doi.org/10.1093/nar/gkx1057>.
- 490 [20] O. Ziv, M.M. Gabryelska, A.T.L. Lun, L.F.R. Gebert, J. Sheu-Gruttaduria, L.W. Meredith,  
491 Z.-Y. Liu, C.K. Kwok, C.-F. Qin, I.J. MacRae, I. Goodfellow, J.C. Marioni, G. Kudla, E.A.  
492 Miska, COMRADES determines in vivo RNA structures and interactions, *Nat. Methods.* 15  
493 (2018) 785–788. <https://doi.org/10.1038/s41592-018-0121-0>.
- 494 [21] S. Lee, F. Kopp, T.-C. Chang, A. Sataluri, B. Chen, S. Sivakumar, H. Yu, Y. Xie, J.T.  
495 Mendell, Noncoding RNA NORAD Regulates Genomic Stability by Sequestering PUMILIO  
496 Proteins, *Cell.* 164 (2016) 69–80. <https://doi.org/10.1016/j.cell.2015.12.017>.
- 497 [22] A. Tichon, N. Gil, Y. Lubelsky, T. Havkin Solomon, D. Lemze, S. Itzkovitz, N.  
498 Stern-Ginossar, I. Ulitsky, A conserved abundant cytoplasmic long noncoding RNA  
499 modulates repression by Pumilio proteins in human cells, *Nat. Commun.* 7 (2016) 12209.  
500 <https://doi.org/10.1038/ncomms12209>.
- 501 [23] X. Wang, J. McLachlan, P.D. Zamore, T.M.T. Hall, Modular recognition of RNA by a human  
502 pumilio-homology domain, *Cell.* 110 (2002) 501–512.  
503 [https://doi.org/10.1016/s0092-8674\(02\)00873-5](https://doi.org/10.1016/s0092-8674(02)00873-5).
- 504 [24] A. Galgano, M. Forrer, L. Jaskiewicz, A. Kanitz, M. Zavolan, A.P. Gerber, Comparative  
505 analysis of mRNA targets for human PUF-family proteins suggests extensive interaction  
506 with the miRNA regulatory system, *PLoS One.* 3 (2008) e3164.  
507 <https://doi.org/10.1371/journal.pone.0003164>.
- 508 [25] Z. Yang, Y. Zhao, G. Lin, X. Zhou, X. Jiang, H. Zhao, Noncoding RNA activated by DNA  
509 damage (NORAD): Biologic function and mechanisms in human cancers, *Clin. Chim. Acta.*



489 (2019) 5–9. <https://doi.org/10.1016/j.cca.2018.11.025>.

[26] N. Soghli, T. Yousefi, M. Abolghasemi, D. Qujeq, NORAD, a critical long non-coding RNA in human cancers, *Life Sci.* 264 (2021) 118665. <https://doi.org/10.1016/j.lfs.2020.118665>.

[27] Y.S. Lee, K. Nakahara, J.W. Pham, K. Kim, Z. He, E.J. Sontheimer, R.W. Carthew, Distinct roles for *Drosophila* Dicer-1 and Dicer-2 in the siRNA/miRNA silencing pathways, *Cell*. 117 (2004) 69–81. [https://doi.org/10.1016/s0092-8674\(04\)00261-2](https://doi.org/10.1016/s0092-8674(04)00261-2).

[28] B.P. Towler, C.I. Jones, S.F. Newbury, Mechanisms of regulation of mature miRNAs, *Biochem. Soc. Trans.* 43 (2015) 1208–1214. <https://doi.org/10.1042/BST20150157>.

[29] R.W. Carthew, E.J. Sontheimer, Origins and Mechanisms of miRNAs and siRNAs, *Cell*. 136 (2009) 642–655. <https://doi.org/10.1016/j.cell.2009.01.035>.

[30] E. Saus, J.R. Willis, L.P. Pryszcz, A. Hafez, C. Llorens, H. Himmelbauer, T. Gabaldón, nextPARS: parallel probing of RNA structures in Illumina, *RNA*. 24 (2018) 609–619. <https://doi.org/10.1261/rna.063073.117>.

[31] Y. Wan, K. Qu, Z. Ouyang, M. Kertesz, J. Li, R. Tibshirani, D.L. Makino, R.C. Nutter, E. Segal, H.Y. Chang, Genome-wide measurement of RNA folding energies, *Mol. Cell*. 48 (2012) 169–181. <https://doi.org/10.1016/j.molcel.2012.08.008>.

[32] Chorostecki U, Willis JR, Saus E and Gabaldon T., Profiling of RNA structure at single-nucleotide resolution using nextPARS, *RNA Bioinformatics*, 978-1-0716-1306-1, 483670\_2\_En, (Chapter 4). In Press. (04-2021).

[33] A. Dobin, C.A. Davis, F. Schlesinger, J. Drenkow, C. Zaleski, S. Jha, P. Batut, M. Chaisson, T.R. Gingeras, STAR: ultrafast universal RNA-seq aligner, *Bioinformatics*. 29 (2013) 15–21. <https://doi.org/10.1093/bioinformatics/bts635>.

[34] J.S. Reuter, D.H. Mathews, RNAstructure: software for RNA secondary structure prediction and analysis, *BMC Bioinformatics*. 11 (2010) 129. <https://doi.org/10.1186/1471-2105-11-129>.

[35] Z. Weinberg, R.R. Breaker, R2R--software to speed the depiction of aesthetic consensus RNA secondary structures, *BMC Bioinformatics*. 12 (2011) 3. <https://doi.org/10.1186/1471-2105-12-3>.

[36] K. Darty, A. Denise, Y. Ponty, VARNA: Interactive drawing and editing of the RNA secondary structure, *Bioinformatics*. 25 (2009) 1974–1975. <https://doi.org/10.1093/bioinformatics/btp250>.

[37] C. Notredame, D.G. Higgins, J. Heringa, T-Coffee: A novel method for fast and accurate multiple sequence alignment, *J. Mol. Biol.* 302 (2000) 205–217. <https://doi.org/10.1006/jmbi.2000.4042>.

[38] E.P. Nawrocki, S.R. Eddy, Infernal 1.1: 100-fold faster RNA homology searches, *Bioinformatics*. 29 (2013) 2933–2935. <https://doi.org/10.1093/bioinformatics/btt509>.

[39] E. Mattei, M. Pietrosanto, F. Ferrè, M. Helmer-Citterich, Web-Beagle: a web server for the alignment of RNA secondary structures, *Nucleic Acids Res.* 43 (2015) W493–7. <https://doi.org/10.1093/nar/gkv489>.

[40] J. Ho, T. Tumkaya, S. Aryal, H. Choi, A. Claridge-Chang, Moving beyond P values: data analysis with estimation graphics, *Nat. Methods*. 16 (2019) 565–566. <https://doi.org/10.1038/s41592-019-0470-3>.

[41] I.V. Novikova, A. Dharap, S.P. Hennesly, K.Y. Sanbonmatsu, 3S: shotgun secondary structure determination of long non-coding RNAs, *Methods*. 63 (2013) 170–177. <https://doi.org/10.1016/j.ymeth.2013.07.030>.

[42] K.E. Lukong, S. Richard, Sam68, the KH domain-containing superSTAR, *Biochimica et Biophysica Acta (BBA) - Reviews on Cancer*. 1653 (2003) 73–86. <https://doi.org/10.1016/j.bbcan.2003.09.001>.

[43] A. Tichon, R.B.-T. Perry, L. Stojic, I. Ulitsky, SAM68 is required for regulation of Pumilio by the NORAD long noncoding RNA, *Genes Dev.* 32 (2018) 70–78.



560 <https://doi.org/10.1101/gad.309138.117>.

561 [44] A. Galarneau, S. Richard, The STAR RNA binding proteins GLD-1, QKI, SAM68 and SLM-2  
562 bind bipartite RNA motifs, *BMC Molecular Biology*. 10 (2009) 47.  
563 <https://doi.org/10.1186/1471-2199-10-47>.

564 [45] M. Feracci, J.N. Foot, S.N. Grellscheid, M. Danilenko, R. Stehle, O. Gonchar, H.-S. Kang,  
565 C. Dalglish, N.H. Meyer, Y. Liu, A. Lahat, M. Sattler, I.C. Eperon, D.J. Elliott, C.  
566 Dominguez, Structural basis of RNA recognition and dimerization by the STAR proteins  
567 T-STAR and Sam68, *Nat. Commun.* 7 (2016) 10355.  
568 <https://doi.org/10.1038/ncomms10355>.

569 [46] Q. Lin, S.J. Taylor, D. Shalloway, Specificity and determinants of Sam68 RNA binding.  
570 Implications for the biological function of K homology domains, *J. Biol. Chem.* 272 (1997)  
571 27274–27280. <https://doi.org/10.1074/jbc.272.43.27274>.

572 [47] A.J. Zaig, T.R. Cech, Analysis of the structure of Tetrahymena nuclear RNAs in vivo:  
573 telomerase RNA, the self-splicing rRNA intron, and U2 snRNA, *RNA*. 1 (1995) 363–374.  
574 <https://www.ncbi.nlm.nih.gov/pubmed/7493315>.

575 [48] J. Tyrrell, K.M. Weeks, G.J. Pielak, Challenge of mimicking the influences of the cellular  
576 environment on RNA structure by PEG-induced macromolecular crowding, *Biochemistry*. 54  
577 (2015) 6447–6453. <https://doi.org/10.1021/acs.biochem.5b00767>.

578 [49] R. Russell, RNA misfolding and the action of chaperones, *Front. Biosci.* 13 (2008) 1–20.  
579 <https://doi.org/10.2741/2557>.

580 [50] Y. Wan, M. Kertesz, R.C. Spitale, E. Segal, H.Y. Chang, Understanding the transcriptome  
581 through RNA structure, *Nat. Rev. Genet.* 12 (2011) 641–655.  
582 <https://doi.org/10.1038/nrg3049>.

583 [51] K.A. Leamy, S.M. Assmann, D.H. Mathews, P.C. Bevilacqua, Bridging the gap between in  
584 vitro and in vivo RNA folding, *Q. Rev. Biophys.* 49 (2016) e10.  
585 <https://doi.org/10.1017/S003358351600007X>.

## 586 Figure legends

### 587 **Figure 1. The landscape of NRUs structures using experimental nextPARS data.**

588 **A.** Overview of the nextPARS experiments. NORAD fragments were probed in three RNA  
589 fragments covering the full-length NORAD lncRNA (overlapping 1903, 1862 and 1614 bases,  
590 respectively), and 11 NRUs with their surrounding regions (overlapping 179 nt each). **B.** On the  
591 top, an arc plot depicting the interactions of the secondary structure inferred from the nextPARS  
592 profiles using RNAstructure software. The core sequences of the NRUs (89nt) are marked  
593 alongside NORAD. On the bottom, the secondary structure of NRUs derived from the full-length  
594 NORAD nextPARS experiment. Scores from full-length NORAD nextPARS profiles are depicted  
595 by colored nucleotides.

596

### 597 **Figure 2. Molecular context provides structural stability to NRUs.**

598 **A.** Overview of nextPARS experiments at three different temperatures: 23 °C, 37 °C and 55 °C.  
599 Arrows showing different comparisons: in grey NRUs compared between those folded in  
600 isolated fragments with larger NORAD fragments, in brown comparison of each NRUs at  
601 different temperatures by pairs, and in blue the comparison of NRUs at different temperatures  
602 by pairs, in the context of the larger NORAD fragments experiments. **B.** On the top, a box plot of  
603 Pearson correlations of the three different comparisons described in A, with individual  
604 observations on top of boxes. On the bottom, a heatmap showing the Pearson correlation  
605 coefficients for each of the comparisons. **C.** Gardner-Altman estimation plot showing the mean  
606 difference between the average of the standard deviation of nextPARS score at the three  
607 different temperatures for the NRUs and for the larger NORAD fragments. Both groups are  
608 plotted on the left axes; the mean difference is plotted on a floating axis on the right as a  
609 bootstrap sampling distribution. The mean difference is depicted as a dot; the 95% confidence  
610 interval is indicated by the ends of the vertical error bar.

611

### 612 **Figure 3. Comparison of positions of SAM68-binding sites against the remaining NRUs** 613 **positions.**

614 **A.** Gardner-Altman estimation plot showing the mean difference between the standard deviation  
615 of nextPARS score at the three different temperatures for SAM68-binding sites positions and the  
616 NRUs remaining positions. Both groups are plotted on the left axes; the mean difference is  
617 plotted on a floating axis on the right as a bootstrap sampling distribution. The mean difference  
618 is depicted as a dot; the 95% confidence interval is indicated by the ends of the vertical error  
619 bar. **B.** A heatmap showing the Pearson correlations coefficients for nextPARS score variability  
620 at different temperatures in positions of UAAA motifs to other positions of NRUs. We show  
621 different correlations for PhastCons score or PhyloP score at different conservation levels, and  
622 using data from isolated NRUs and NRUs in the context of larger NORAD fragments.

623

624

### 625 **Figure 4. Comparison of alternative structures of NRUs and obtained consensus** 626 **structure.**

627 **A.** The consensus secondary structure for the core region of NRUs, derived by using a multiple  
 628 sequence alignment to derive a from the eight NRUs that have a clear conserved long  
 629 stem-loop hairpin (NRU#1, NRU#3-8 and NRU#10). **B.** Secondary structure conformations A  
 630 and B, from NRU#2 obtained using Rsample software in combination with nextPARS from larger  
 631 NORAD fragments experiments. Scores from nextPARS scores are depicted by colored  
 632 nucleotides. Known structural and sequence motifs are marked in the conformation A. **C.** A box  
 633 plot showing the structural similarity (Beagle's z-score) elements found by Beagle software, for  
 634 the structure ensemble alignment and for the most stable structure alignment.

635

636 **Figure 5. Discovery of two previously uncharacterized NRUs.**

637 **A.** Overview of the relative positions of the core sequence of the NRUs along with NORAD. The  
 638 core positions of previously characterized NRUs are marked with grey bars, and the two new  
 639 NRUs (NRU#10a and NRU#10b) are marked with green bars. The nextPARS score derived  
 640 from the larger NORAD fragments experiment is shown, by an average window of 10nt.  
 641 SAM68-binding sites are marked with brown lines. PhastCons score (based on the 100-way  
 642 vertebrate alignment) is shown at the bottom. **B.** On the top, secondary structures of NRU#10a  
 643 and NRU#10b. On the bottom the sequence of NRU#10a and NRU#10b and the PhyloP score  
 644 (based on the 100-way vertebrate alignment). Known structural and sequence motifs are  
 645 marked in the sequence and in the structure.

# Figure 1

bioRxiv preprint doi: <https://doi.org/10.1101/2021.03.29.437547>; this version posted March 30, 2021. The copyright holder for this preprint (which was not certified by peer review) is the author/funder. All rights reserved. No reuse allowed without permission.

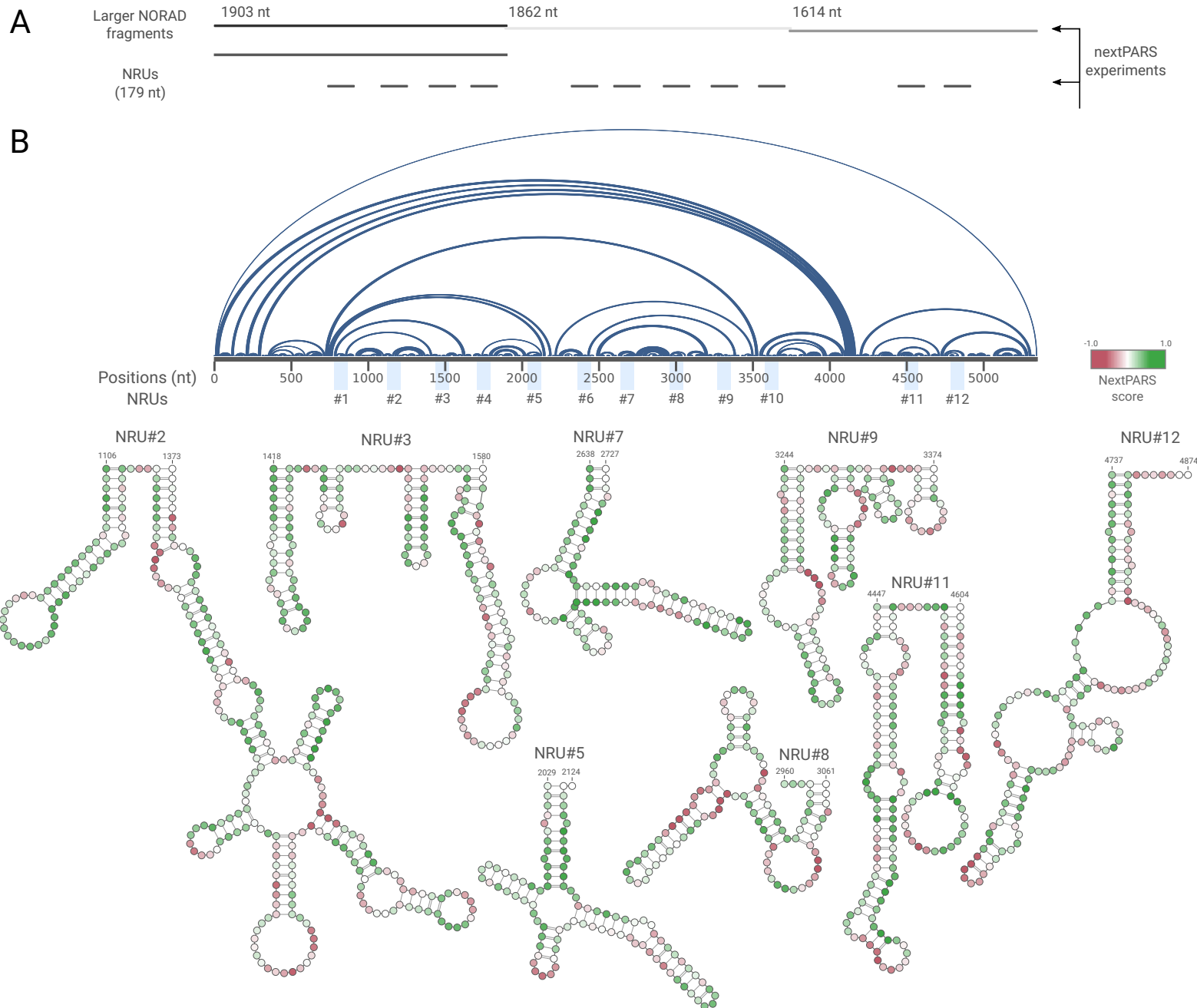
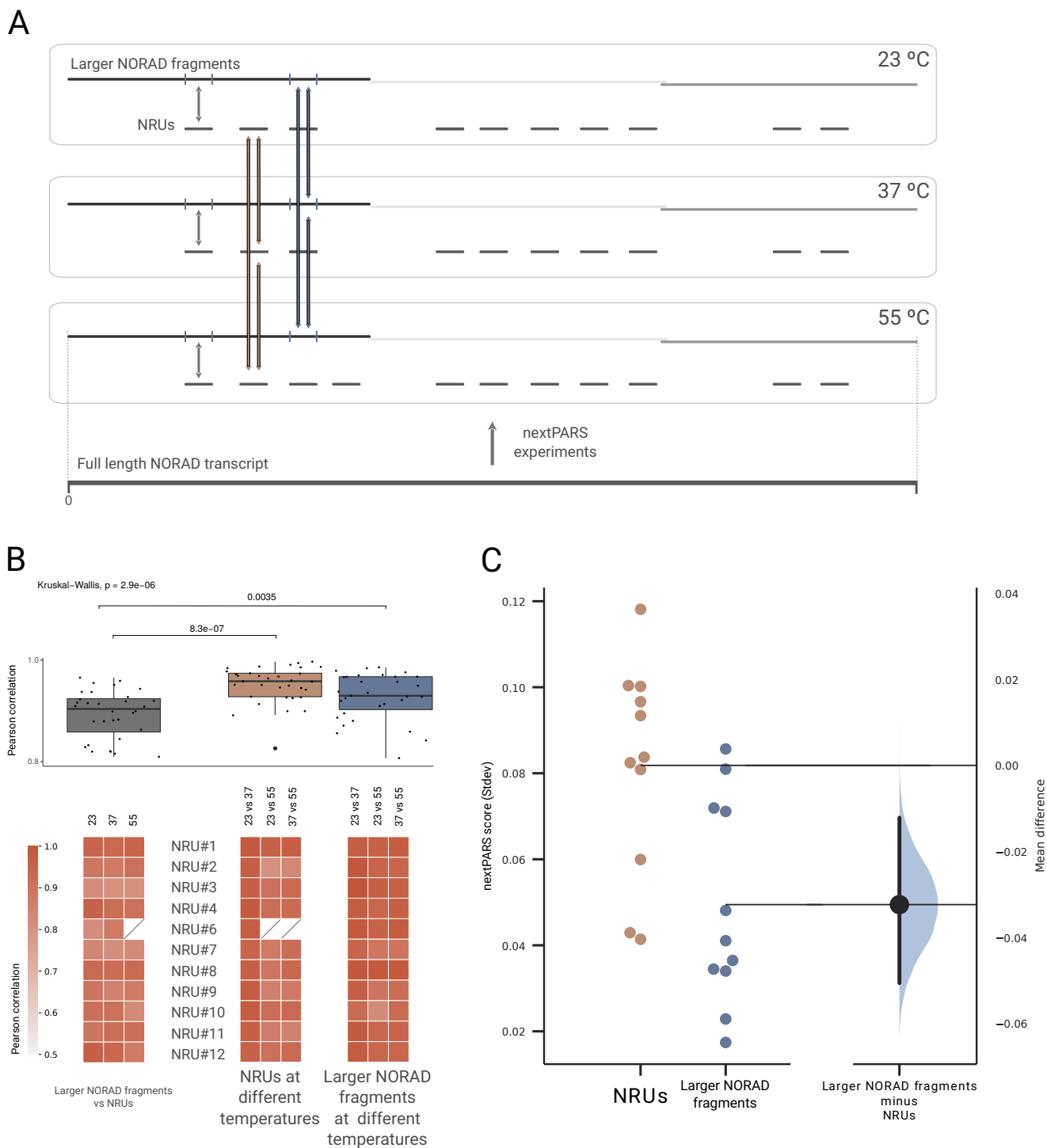
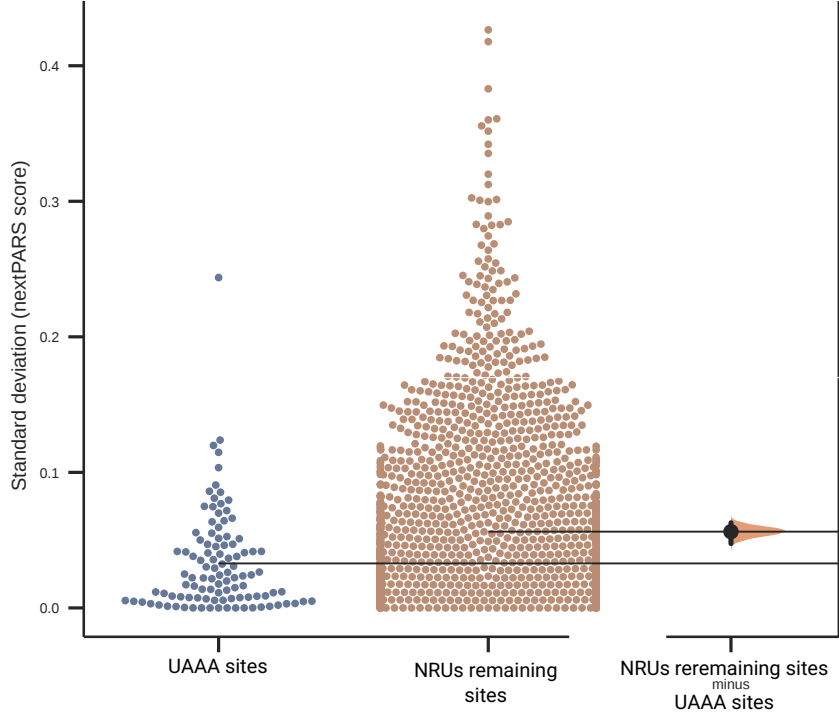


Figure 2  
bioRxiv preprint doi: <https://doi.org/10.1101/2021.03.29.437547>; this version posted March 30, 2021. The copyright holder for this preprint (which was not certified by peer review) is the author/funder. All rights reserved. No reuse allowed without permission.





A



B

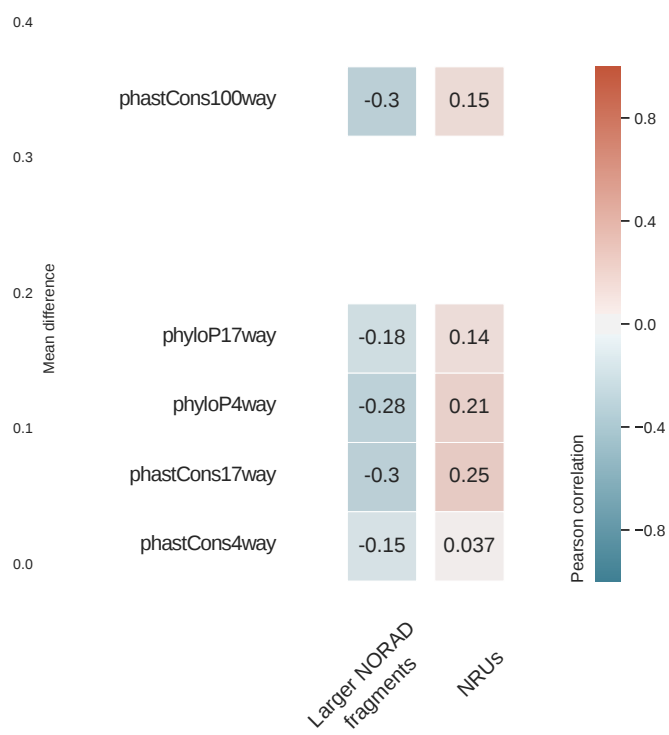
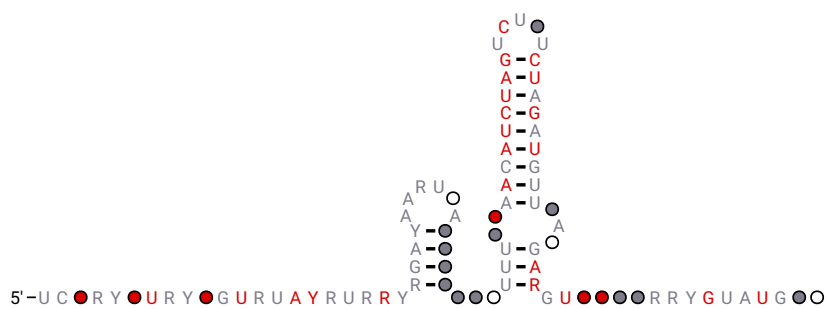


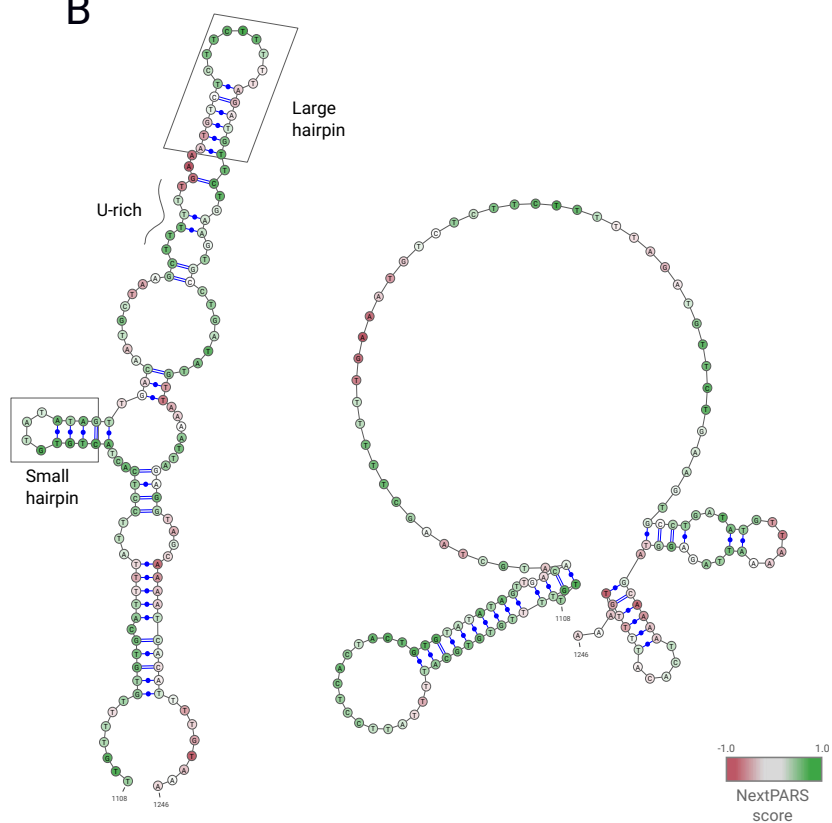
## Figure 4

bioRxiv preprint doi: <https://doi.org/10.1101/2021.03.29.437547>; this version posted March 30, 2021. The copyright holder for this preprint (which was not certified by peer review) is the author/funder. All rights reserved. No reuse allowed without permission.

A



B



Conformation A  
84.1%

Conformation B  
15.9%

C

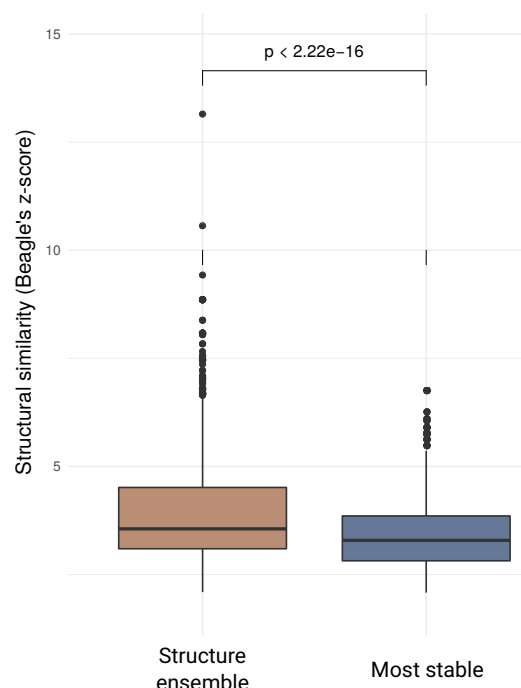
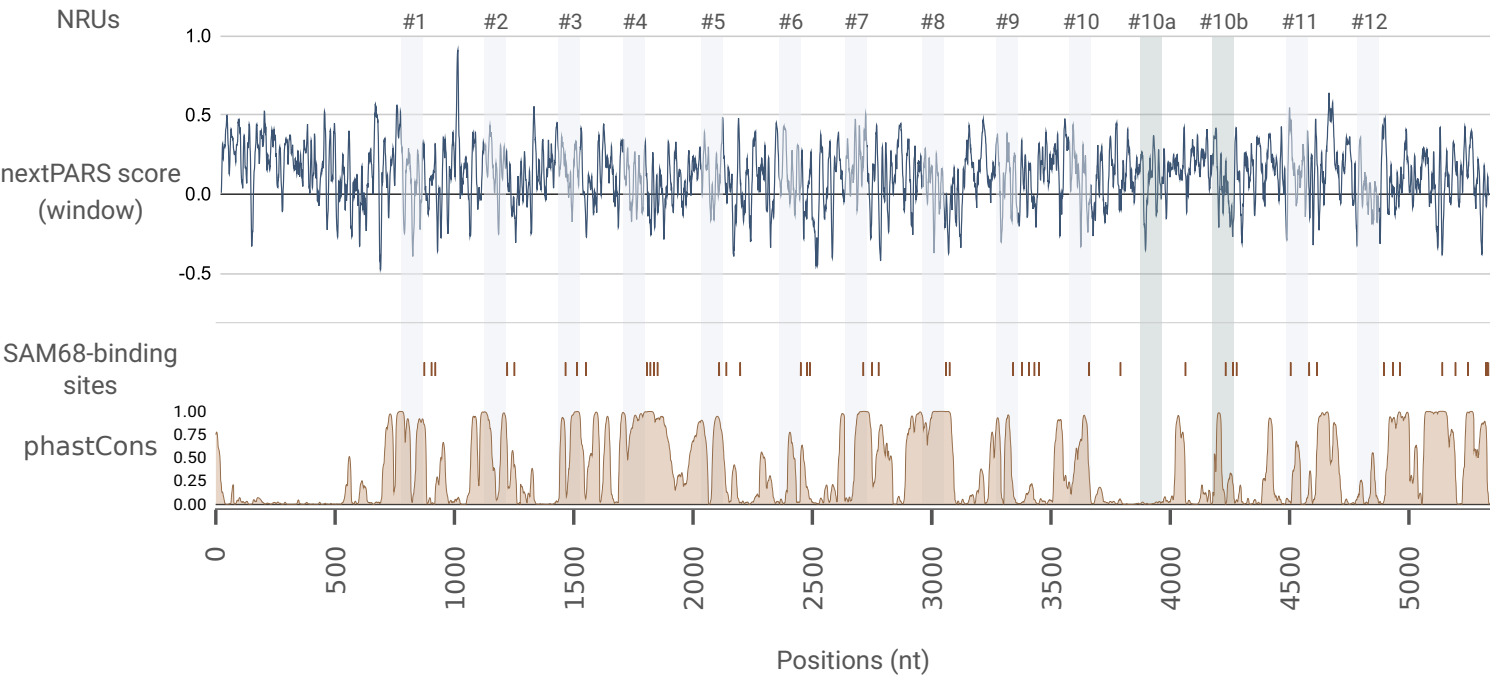


Figure 5

A

bioRxiv preprint doi: <https://doi.org/10.1101/2021.03.29.437547>; this version posted March 30, 2021. The copyright holder for this preprint (which was not certified by peer review) is the author/funder. All rights reserved. No reuse allowed without permission.



B

